

Thermally Driven Exchanges between a Coral Reef and the Adjoining Ocean

STEPHEN G. MONISMITH

Environmental Fluid Mechanics Laboratory, Stanford University, Stanford, California

AMATZIA GENIN

H. Steinitz Marine Biological Laboratory, Interuniversity Institute for Marine Science, The Hebrew University, Eilat, Israel

MATTHEW A. REIDENBACH*

Environmental Fluid Mechanics Laboratory, Stanford University, Stanford, California

GITAI YAHIEL[†]

H. Steinitz Marine Biological Laboratory, Interuniversity Institute for Marine Science, The Hebrew University, Eilat, Israel

JEFFREY R. KOSEFF

Environmental Fluid Mechanics Laboratory, Stanford University, Stanford, California

(Manuscript received 27 June 2005, in final form 18 November 2005)

ABSTRACT

In this paper hydrographic observations made over a fringing coral reef at the northern end of the Gulf of Aqaba near Eilat, Israel, are discussed. These data show exchange flows driven by the onshore–offshore temperature gradients that develop because shallow regions near shore experience larger temperature changes than do deeper regions offshore when subjected to the same rate of heating or cooling. Under heating conditions, the resulting vertically sheared exchange flow is offshore at the surface and onshore at depth, whereas when cooling dominates, the pattern is reversed. For summer conditions, heating and cooling are both important and a diurnally reversing exchange flow is observed. During winter conditions, heating occupies a relatively small fraction of the day, and only the cooling flow is observed. When scaled by ΔV , the observed profiles of the cross-shore during cooling velocity collapse onto a single curve. The value of ΔV depends on the convective velocity scale u_f and the bottom slope β through the inertial scaling, $\Delta V \sim \beta^{-1/3} u_f$ first proposed by Phillips in the 1960s as a model of buoyancy-driven flow in the Red Sea. However, it is found that turbulent stresses associated with the longshore tidal flows and unsteadiness due to the periodic nature of the buoyancy forcing can act to weaken the sheared exchange flow. Nonetheless, the measured exchange flow transport agrees well with previous field and laboratory work. The paper is concluded by noting that the “thermal siphon” observed on the Eilat reef may be a relatively generic feature of the nearshore physical oceanography of reefs and coastal oceans in general.

1. Introduction

Coral reefs are known to draw nutrients, zooplankton, and phytoplankton from the surrounding waters

(Baird and Atkinson 1997; Yahel et al. 1998), implying that the functioning of reef communities might be strongly influenced by the hydrodynamic supply of materials to the reef (Hatcher 1997). While recycling of materials within the reef is important, hydrodynamic processes govern the net loss or gain of material, as well as the dispersal and recruitment of larval organisms from and to the reef.

However, in many reef systems, Eulerian mean currents are weak [e.g., Kaneohe Bay away from the reef crest; see Falter (2003)] or, excepting a few well-defined channels, are parallel to reef topography. Mechanisms for cross-shore exchange, that is, exchange between the

* Current affiliation: Department of Civil and Environmental Engineering, University of California, Berkeley, Berkeley, California.

[†] Current affiliation: Department of Biology, University of Victoria, Victoria, British Columbia, Canada.

Corresponding author address: S. G. Monismith, Environmental Fluid Mechanics Laboratory, Stanford University, Stanford, CA 94305-4020.

E-mail: monismith@stanford.edu

reef and the adjoining ocean, include forcing by surface and internal waves (e.g., Munk et al. 1949; Leichter et al. 1996), divergence of longshore flows by variations in roughness (Gross and Werner 1994), boundary mixing (see Wolanski 1987), and convective flows (Boden 1952). For example, pioneering studies by von Arx (1954) and Munk et al. (1949) examined flushing of reef lagoons, focusing on exchanges forced either by wave-driven flows over the fringing reef or by wind-driven or tidal flows through passages in the reef (Atkinson et al. 1981). More recent work has examined wave transformation and wave forcing of flows over and along fringing reefs (Symmonds et al. 1995; Hearn 1999; Lugo-Fernandez et al. 1998; Kraines et al. 1998; Lowe et al. 2005). Leichter et al. (1996; 2003) document how shoaling of internal waves can be important to the cross-shore exchange of water on a fringing reef off the Florida Keys.

In this paper we will present observations of exchange flows forced by temperature differences that develop between a coral reef and the adjacent ocean because of variations in depth. Monismith et al. (1990) present observations of this process in a small reservoir, showing how nighttime cooling of the reservoir led to offshore flows from a shallow sidearm of the reservoir into the deeper main body of the reservoir, with a compensating surface inflow into the sidearm (see also Sturman et al. 1999). During daytime heating, the opposite took place, with warm surface waters leaving the sidearm being replaced by cooler deeper water from the reservoir.

The operation of a similar thermal mechanism over coral reefs was identified some years ago by Boden (1952), who observed that the lagoon defined by Bermuda and its system of reefs was 0.2°C warmer than the nearby Atlantic Ocean. Checkley et al. (1988) hypothesized that a similar mechanism is important to Atlantic menhaden recruitment on the mid-Atlantic coast. Symonds and Gardiner-Garden (1994) showed how cooling can drive exchanges between a coastal embayment and the waters of the East Australian continental shelf. As discussed in Symonds and Gardiner-Garden (1994), there is an important issue of scale inherent to all these observations. For example, the lens of warm salty water formed in the Bermuda lagoon is in geostrophic balance and circulates anticyclonically, with offshore spreading of the lens inhibited by rotation (Symonds and Gardiner-Garden 1994; Jacobs and Ivey 1999). Moreover, such a density front can be baroclinically unstable, with the offshore flux of heat and mass from the lagoon being effected by eddies rather than by estuarine-like buoyancy-driven flows (see Pringle 2001).

However, in the region closest to the shore, that is,

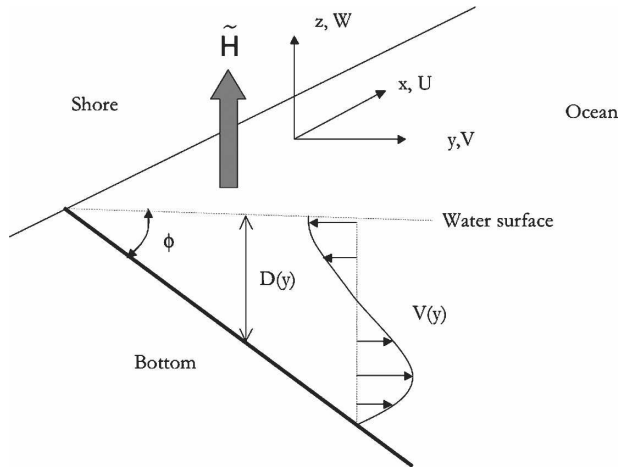


FIG. 1. Sketch of problem geometry for heating and cooling flows in a wedge.

well within one internal Rossby radius of the coast (perhaps less than 1 km), rotational effects will be small, and direct offshore buoyancy-driven transport may dominate. We note that despite the ecological significance of this region (not just for coral reefs), and excepting studies of flows near beaches (e.g., Lentz et al. 1999), there are few reports of flows or transport mechanisms close to the coast [see Storlazzi et al. (2003) for a rare exception], that is, where rotation is not important.

In the sections below we start by analyzing the mechanics of these thermally driven flows. This analysis serves as a basis for interpreting the hydrodynamic data we will present. We conclude by discussing the applicability of our results to other coral reef geometries and forcing conditions.

2. Background

The basic mechanism underlying the “thermal siphon” is that horizontal temperature differences develop where the water depth D varies (Farrow and Patterson 1993). For example, neglecting (for now) advection of heat, the thermal energy equation, written in integrated form for a water column of depth D that varies with distance from the shore y in the presence of a total surface heat flux \tilde{H} (positive outward), is (Fig. 1)

$$\frac{\partial \bar{\theta}}{\partial t} = - \frac{\tilde{H}}{\rho_0 c_p D(y)}, \tag{1}$$

where $\bar{\theta}$ is the depth-averaged temperature, c_p is the heat capacity at constant pressure (4.2 KJ kg⁻¹ K), and $\rho_0 = 1000 \text{ kg m}^{-3}$ is the reference density of water. In writing (1) we have assumed that all of the incident

shortwave radiation is absorbed in the water column. According to (1), we expect shallow regions (small D) to heat or cool much more rapidly than do deep regions (large D).

How the flow evolves in response to this imposed heat flux depends on the bottom slope, the strength of the forcing, and the periodicity of the forcing. Farrow and Patterson (1993) considered periodic heating and cooling of fluid in a wedge, finding via perturbation analysis that if the slope is small, advection of heat and momentum can be neglected allowing analytical solutions to be developed. The nature of the response depends on the local depth: the shallowest waters respond in an entirely viscous fashion whereas the deepest waters remain inertial. The transition depth D_t for the wedge is found by computation and scaling to be

$$D_t \sim 0.3qT, \quad (2)$$

where $T = 24$ h is the period of the heating-cooling cycle and q is the appropriate turbulent velocity scale. Equation (2) is based on the assumption that the eddy viscosity can be written as $\nu_t \sim qD$. For convection,

$$q = u_f = \left(\frac{\alpha g D \tilde{H}_0}{\rho_0 c_p} \right)^{1/3}, \quad (3)$$

where the convective velocity scale u_f is defined in terms of \tilde{H} , D , the heat capacity at constant pressure c_p , and the reference density $\rho_0 = 1000 \text{ kg m}^{-3}$ (Fischer et al. 1979).

For $D < D_t$ (i.e., inshore) the viscous flow is found to be (see also the appendix)

$$V_{VU} \sim \frac{\beta u_f^3 T}{qD} \quad (4)$$

or, for pure convection,

$$V_{VU} \sim \frac{\beta u_f^2 T}{D}. \quad (5)$$

For $D > D_t$, the flow lags the forcing by $T/4$ and scales as

$$V_{UU} \sim \frac{\beta u_f^3 T^2}{D_0^2}. \quad (6)$$

In (4)–(6) we have used subscripts to indicate both the type of momentum balance (unsteady inertia or viscous) and the thermal energy balance (unsteady). Note that the unsteady balance given in (1) is fundamental to Farrow and Patterson's analysis. While Farrow and Patterson's analysis neglected advective inertia, it is simple to construct a third scaling based on a nonlinear (N) inertia–buoyancy balance that still uses (1). That is, if

$$V \frac{\partial V}{\partial y} \sim \frac{1}{\rho_0} \frac{\partial P}{\partial y} \sim \alpha g \frac{\partial \bar{\theta}}{\partial y} D, \quad (7)$$

then a third possibility is

$$V_{NU} \sim \left(\frac{u_f^3 T}{D} \right)^{1/2}. \quad (8)$$

As the thermal flow spins up, advection of heat may become important. In this case, we can construct a second set of scalings analogous to (4)–(8). If we suppose that advection of heat balances the local heating, that is, a steady thermal balance

$$V \frac{\partial \theta}{\partial y} \sim \frac{\tilde{H}}{\rho_0 c_p D}, \quad (9)$$

we find that

$$V_{NS} \sim \beta^{-1/3} u_f, \quad (10)$$

$$V_{VS} \sim \frac{u_f^{3/2}}{q^{1/2}}, \quad (11)$$

and

$$V_{US} \sim \left(\frac{u_f^3 T}{D} \right)^{1/2}. \quad (12)$$

The steady balances for momentum and heat that give (10) are the same ones used by Phillips (1966) in his model of buoyancy-driven flow in the Red Sea (see also Tragou and Garrett 1997). Indeed, since $D = \beta y$, we could write (10) as $V_{NS} \sim (B_0 y)^{1/3}$ where $B_0 = (\alpha g \tilde{H} D / \rho_0 c_p)$ is the surface buoyancy flux; that is, V_{NS} is the Phillips scale for the convective flow. Expressed in terms of the total exchange flow, $Q \sim V_{NS} D$, this result is similar to that of Sturman et al. (1999) who found from laboratory experiment and by reanalysis of previous field data that

$$Q = 0.24 u_f H \left(\frac{1}{1 + \beta} \right)^{4/3}. \quad (13)$$

The constant of proportionality in (13) was derived by fitting laboratory and field observations. It should be noted that Sturman et al. (1999) considered the cooling to be applied to a limited region of the wedge; in their analysis, the extra dependency on β appears because of the inshore growth of the convecting layer from the edge where cooling is imposed. In contrast, in the field observations we present the cooling is effectively of infinite offshore extent.

Further consideration of the scalings above is given in the appendix, where we also derive conditions for the applicability of the different balances. These scaling arguments suggest that diurnally reversing thermally driven flows with a magnitude determined primarily by

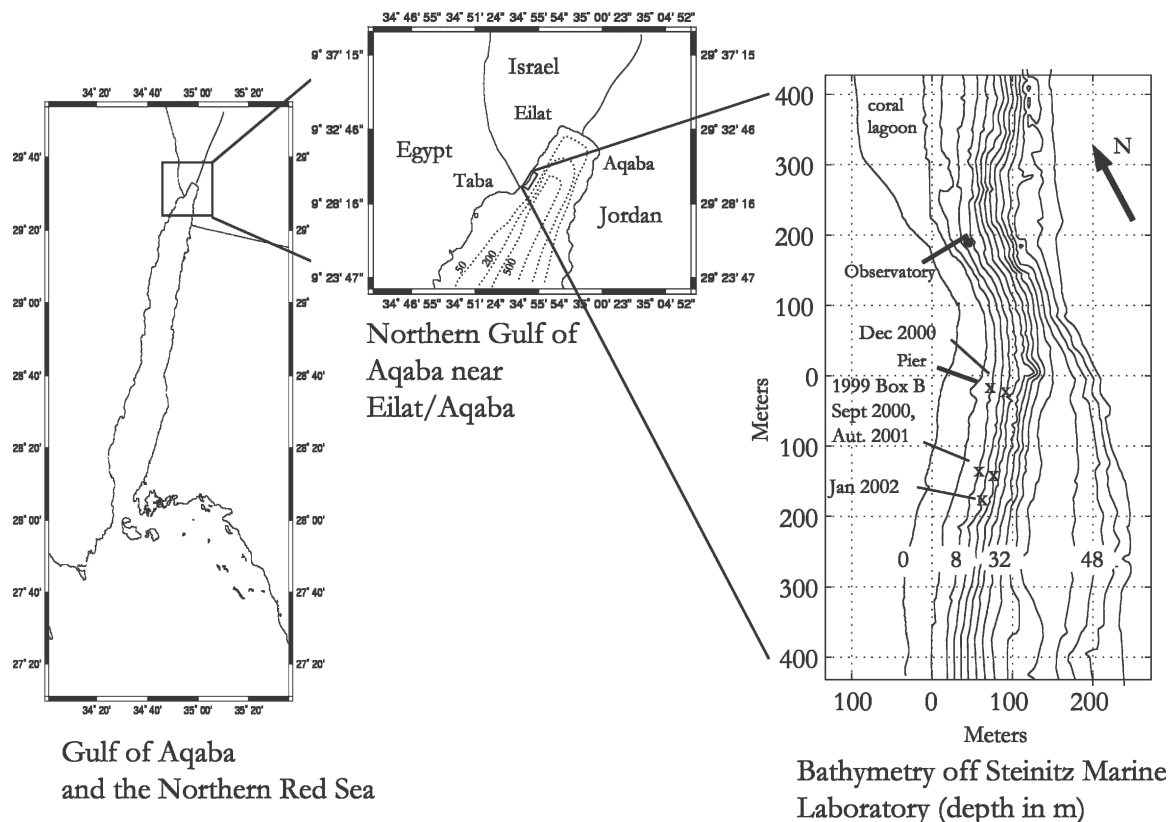


FIG. 2. Map of the Eilat region with bathymetry showing different instrument deployment locations.

the strength of the buoyancy forcing should be a persistent feature of flows over a sloping bottom like that found for the fringing reef at Eilat. The scaling also suggests that the presence of longshore flows driven by barotropic pressure gradients can weaken these gravitational exchanges by increasing the vertical mixing of momentum. In what follows, we show that this picture is indeed correct, with the scaling coefficient appearing in (13) similar to but larger than the value determined from laboratory experiments, albeit with a dependence on parameters that represent the effects of turbulence produced by the longshore tidal flows and the unsteadiness of the buoyancy forcing.

3. Methods

Our experiments were carried out on the nearshore reef adjacent to the Steinitz Marine Laboratory in Eilat, Israel. This fringing reef, with its coral cover extending from the shore to approximately 100-m depth, is typical in structure to many of the reefs of the Red Sea (see e.g., Fishelson 1971; Benayahu and Loya 1977; Yahel et al. 2002). The bathymetry of the site and the northern end of the Gulf of Aqaba (Eilat) are shown in

Fig. 2. Typical flows at this site range from 5 to 30 cm s^{-1} and are predominantly directed along isobaths (Genin and Paldor 1998; Monismith and Genin 2004). Local winds mainly come from the north such that wind stresses directed in the cross-shore direction are generally small. Reflecting the fact that the response of the gulf to winds is largely at the scale of the whole basin [e.g., upwelling and gyres; cf. Berman et al. (2000)], we note at the outset that we did not find any relation between winds and the exchange flows we observed, except to the extent that higher wind speeds were generally associated with more evaporation and hence larger values of u_r .

As part of an overall project examining benthic grazing by coral reefs, we carried out a series of experiments measuring flows over the Eilat reef. During the first experiment, which took place from 27 August to 14 September 1999 (see Genin et al. 2002), we deployed an upward-looking 600-kHz RDI workhorse ADCP at three different positions, over corals at 8- and 15-m depths, and over a nearby sandy region in 15 m of water. These positions are marked in Fig. 2. For these deployments we used 50-cm bins and acquired velocities at 2 Hz. During a second experiment, which took

place in December 2000–January 2001, we deployed a 600-kHz ADCP on the 16-m isobath.¹ During the third experiment, which took place from 19 September 2001 to 12 November 2001, we deployed one 600-kHz ADCP on the 8-m isobath and a second on the 16-m isobath along with two pairs of SBE 39 thermistor loggers and a Seabird SBE19 Seacat CTD. During the last experiment, a second grazing experiment carried out in early January 2002, we deployed two upward-looking 600-kHz ADCPs (1-m bins) 30 m apart, each in 14 m of water, along with a Nortek 1.5-MHz ADP operating in its coherent mode [3-cm bins; see Gordon et al. (1998)] looking down from 2 m above the bottom in 12 m of water.

In addition to fixed instruments, during all experiments we made sporadic measurements of temperature and salinity variability using an Applied Microsystems CTD. The CTD was used either to measure vertical profiles or, by swimming with the CTD held on the surface, the offshore structure of the near-surface temperature field.

To compute surface heat fluxes, we used 15-min meteorological data routinely acquired at the Steinitz laboratory. Available data include wind speed and direction, humidity, air temperature, sea surface temperature, atmospheric pressure, and incoming shortwave radiation. These data were used with the air–sea interaction algorithms presented in Fairall et al. (1996) and given in the Matlab Air–Sea toolbox [developed by S. Lentz, R. Beardsley, and R. Pawlowicz; see Pawlowicz et al. (2001)] to compute the latent, sensible, and net longwave heat fluxes. Because detailed data on cloud fraction were not available, and given that the measured shortwave radiation generally matched well with appropriate clear-sky values (a reasonable assumption given that Eilat has on average 300 cloudless days per year), we computed the net longwave flux assuming that the sky was always clear. To convert these fluxes into an estimate of temperature changes due to surface heat exchanges, we assumed (a) either a constant mixed layer depth or a mixed layer depth that varied linearly with time during periods of extended cooling (e.g., autumn 2001) and (b) that there was an entrainment flux equal to 30% of the net surface heat exchanges (Spigel et al. 1986). This is a simplified version of the mixed layer model given in Wolf-Vecht et al. (1992). Given the uncertainty in the latent (and possibly sensible) heat fluxes, further refinement did not seem warranted at this time.

¹ These data were primarily collected by Dr. T. Berman as part of the USAID-sponsored Red Sea Peace Park. We gratefully acknowledge his making these data available to us.

In comparing observed and computed surface temperatures, we found that it was necessary to increase the computed latent heat flux by a factor of 2.3 to match the observed cooling. This value was not chosen at random; instead, we based our choice on the fact that the original computed latent heat flux corresponded to an evaporation rate of 4 mm day^{-1} . However, observations (Assaf and Kessler 1976) show that the real evaporation rate for the Gulf of Eilat is approximately 1 cm day^{-1} on average.

4. Observations

The observations we present below show two types of thermally driven flows: during periods of net heating of the water column the exchange flow cycles diurnally with offshore flows at the surface during the day and at depth at night, while during periods of net cooling, we largely see only offshore flows at depth. Two of our ADCP deployments are discussed below.

a. August–September 1999: Heating and cooling

Genin et al. (2002) and Reidenbach (2004) describe salient features of the experiment pertinent to measurements of near-bottom turbulence and phytoplankton depletion by reef grazing. As seen in Fig. 3a, during this experiment there were persistent diurnal winds blowing down the gulf (direction not shown in figure), a condition commonly found in summer in Eilat (Berman et al. 2003). The average wind speed over this period of time was 4.6 m s^{-1} . Since the Rossby radius of deformation was slightly less than the width of the gulf, these winds should have led to a large-scale downwelling on the western shore of the gulf (Berman et al. 2000). This was seen in a drop of the nearshore thermocline by 25 m between 30 August and 3 September.

Heating of the water by incident shortwave radiation was generally less than was cooling by the sum of the other heat fluxes, with cooling dominated by latent heat fluxes associated with the winds and the low relative humidity of the air in Eilat. As seen in Fig. 3d, nighttime cooling rates as large as 400 W m^{-2} were not uncommon. In agreement with temperature changes computed from a heat balance over a 20-m mixed layer, during the period of the main ADCP deployments we show below, the surface temperature dropped several degrees over this period (Fig. 3f). Throughout the ADCP deployments (days 240–255), the period of cooling was a larger fraction of the day (0.6) than was the period of net heating (0.4). As seen at the shallow-water station in box B (days 245–250), this diurnal cycle of heating and cooling (Fig. 4a) results in a diurnal cycle of vertically sheared offshore exchange flows (Fig. 4c)

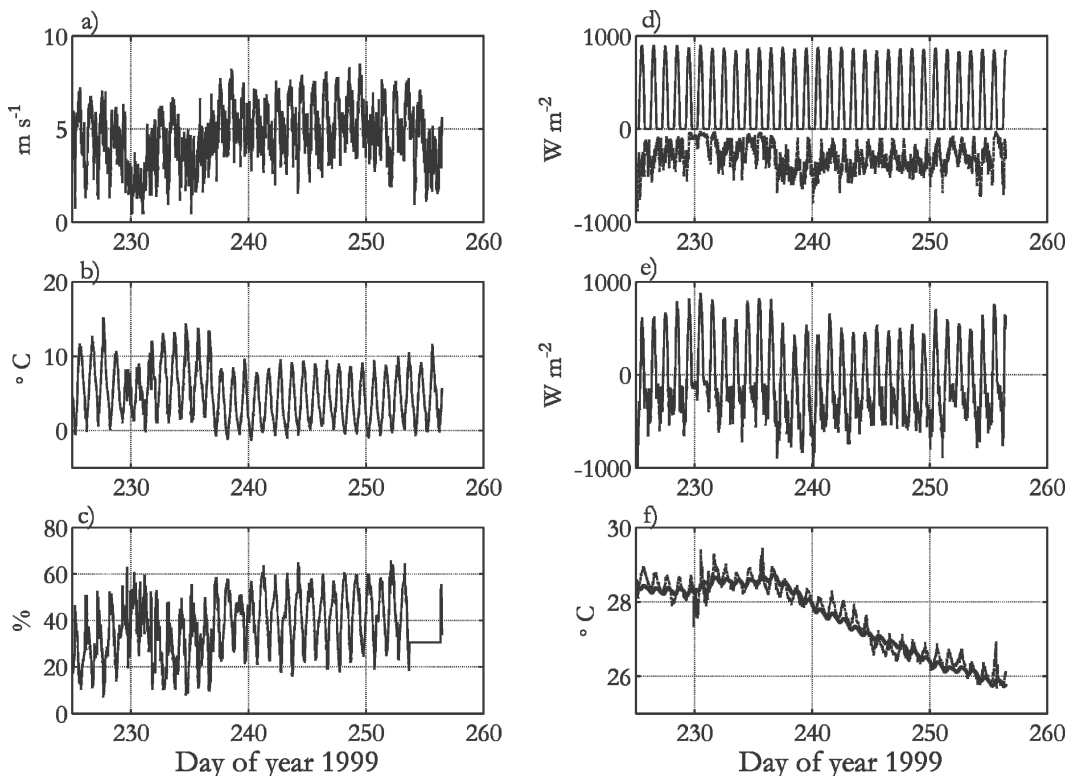


FIG. 3. Meteorological conditions August–September 1999: (a) wind speed; (b) air–sea temperature difference; (c) relative humidity; (d) surface heat fluxes due to shortwave radiation (solid line) and cooling by net longwave radiation, evaporation, and sensible heat flux (dashed line); (e) total surface heat flux; and (f) observed (dotted line) and modeled (solid line) water surface temperature. Note that in (f) the observed temperature shows diurnal variations that reflect the difference between average mixed layer temperature and the water surface temperature.

with sustained peak velocities of 3 cm s^{-1} . These diurnal exchange flows were not locked to the semidiurnal longshore tidal flows (Fig. 4b). Since for both the heating and cooling periods the outflow was about 3 m deep, we estimate that the exchange flows were approximately $0.03 \text{ m}^2 \text{ s}^{-2}$. This gives a flushing time for waters shoreward of the ADCP of about $300 \text{ m}^2 \cdot 0.03 \text{ m}^2 \text{ s}^{-1} \approx 3 \text{ h}$.

Last, there appears to be a time lag of about 2 h between the onset of cooling and the appearance of the developed cooling flow, whereas the lag between the shift from cooling to heating to the appearance of the heating flow is nearly zero. The existence of some lag between the change of the sign of the heat flux and the changing of direction of the exchange flow is expected given that the preexisting flow must be decelerated and its concomitant temperature gradient wiped out before the new flow can be spun up (Farrow and Patterson 1993). However, at the end of the heating phase, there will also be a weak near-surface thermal stratification that first must be mixed out before the cooling flow can develop. In contrast, at the end of the cooling phase the water column is well mixed, and whatever small lag

there is to be observed is likely due only to arresting the cooling flow and spinning up the heating flow. Thus, the difference in behavior between heating and cooling must reflect the extra time required to first eliminate the preexisting stratification before flow reversal can take place and the cooling flow becomes established.

b. September–November 2001

For the first 10 days of this experiment the daily averaged temperature was roughly constant whereas for the remaining 27 days the temperature dropped significantly (Fig. 5a), reflecting the persistent cooling that is experienced in the Gulf of Aqaba in autumn and winter (Wolf-Vecht et al. 1992). As a result, during this initial period, the entire water column stratified diurnally. In contrast, during the later cooling period, only very weak stratification developed near the surface (Fig. 5b). Between 2 September and 11 November 2001 the mixed layer deepened from about 20 m to approximately 100 m (Monismith and Genin 2004). Despite the fact that this experiment was largely done during a period of net cooling, and the cross-shore flow was mostly offshore at the bottom, the offshore surface flow during

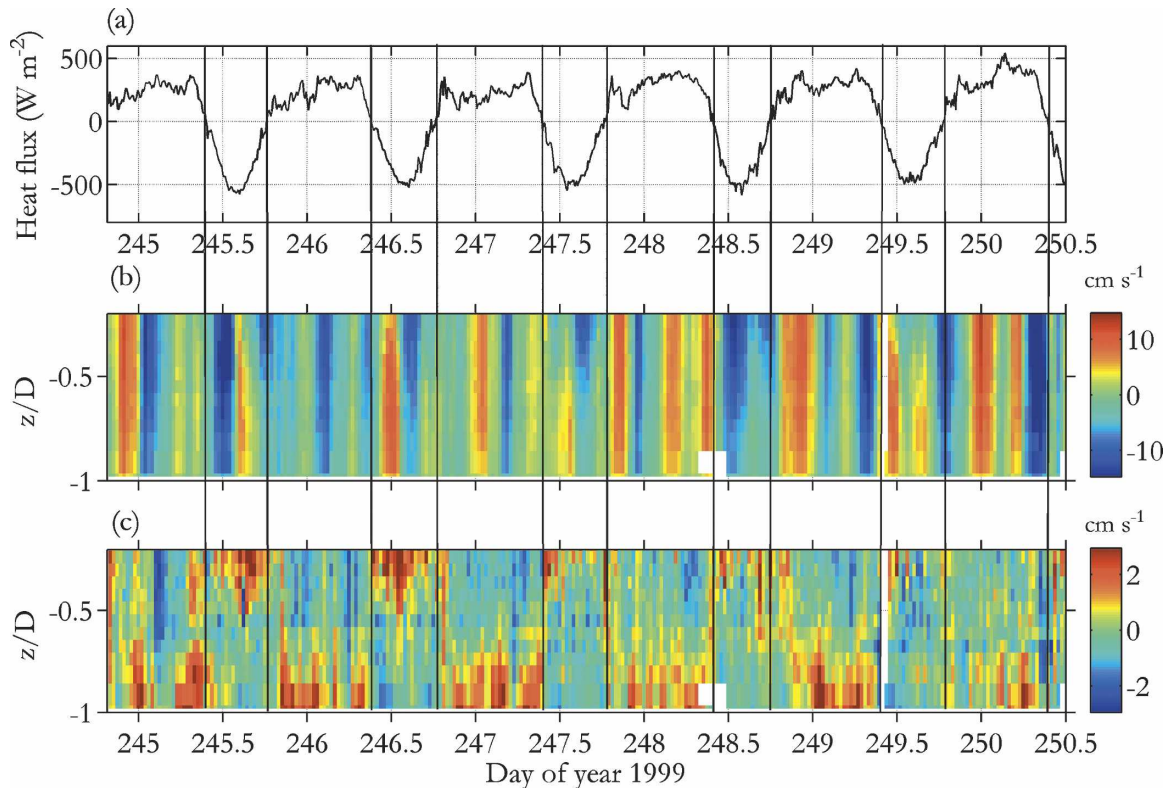


FIG. 4. Box-B observations: (a) surface heat flux, (b) longshore flow on the 8-m isobath, and (c) cross-shore flow on the 8-m isobath. The vertical lines mark the transitions from heating to cooling and vice versa.

daytime heating, and thus the diurnally reversing exchange flow, were still apparent (Figs. 5c and 5d). Overall the top–bottom shear in the cross-shore velocity pulsed diurnally from 2 cm s^{-1} offshore at the surface to a maximum strength of 5 cm s^{-1} offshore at the bottom.

Throughout this period, the longshore flow varied semidiurnally as well as fortnightly. Interestingly, the strongest exchange flows did not obviously correspond to the weakest longshore flows, or as is shown in Fig. 6a, the weakest bottom stress, or the strongest cooling (Fig. 6b), although clear differences in cross-flow strength can be seen between the times when the surface temperature was decreasing (days 270–275 and 288–310) and when it was increasing (days 268–270 and 275–288). We will return to this question of the scaling below when we synthesize all of the observations.

The horizontal difference in temperature at 8-m depth between the 8- and 16-m water columns (Fig. 6c) shows the persistent cycle of horizontal temperature gradients expected for differential heating and cooling. This confirms the fundamental basis of the thermal cycling mechanism—that of horizontal temperature variations forced by bathymetry. Close examination of the relative phasing of the surface heating and the horizon-

tal temperature gradient shows that they are nearly in phase, except when the flow is switching from heating to cooling. As a consequence, the horizontal temperature difference appears to depend primarily of the instantaneous surface heat flux (Fig. 7). According to (9), this indicates that primary thermal energy balance must be between cross-shore advection of heat and local heating.

5. Synthesis

The general behavior of both the cooling and heating flows is best illustrated by the August 1999 box-B data. To examine the vertical structure of these flows, we formed composite profiles of the heating and cooling period flows for the box-B data as follows. We first averaged the velocity at each depth separately for each period in which the flow was either in the heating or cooling flow pattern. Each of these was then normalized by its respective average value of the top–bottom shear, ΔV . As seen in Fig. 8, remarkably, aside from the bottom boundary layers, the heating and cooling flows were nearly mirror images of each other in the sense that the vertical structure of the heating flow was close to being an inversion of that of the cooling flow. Pre-

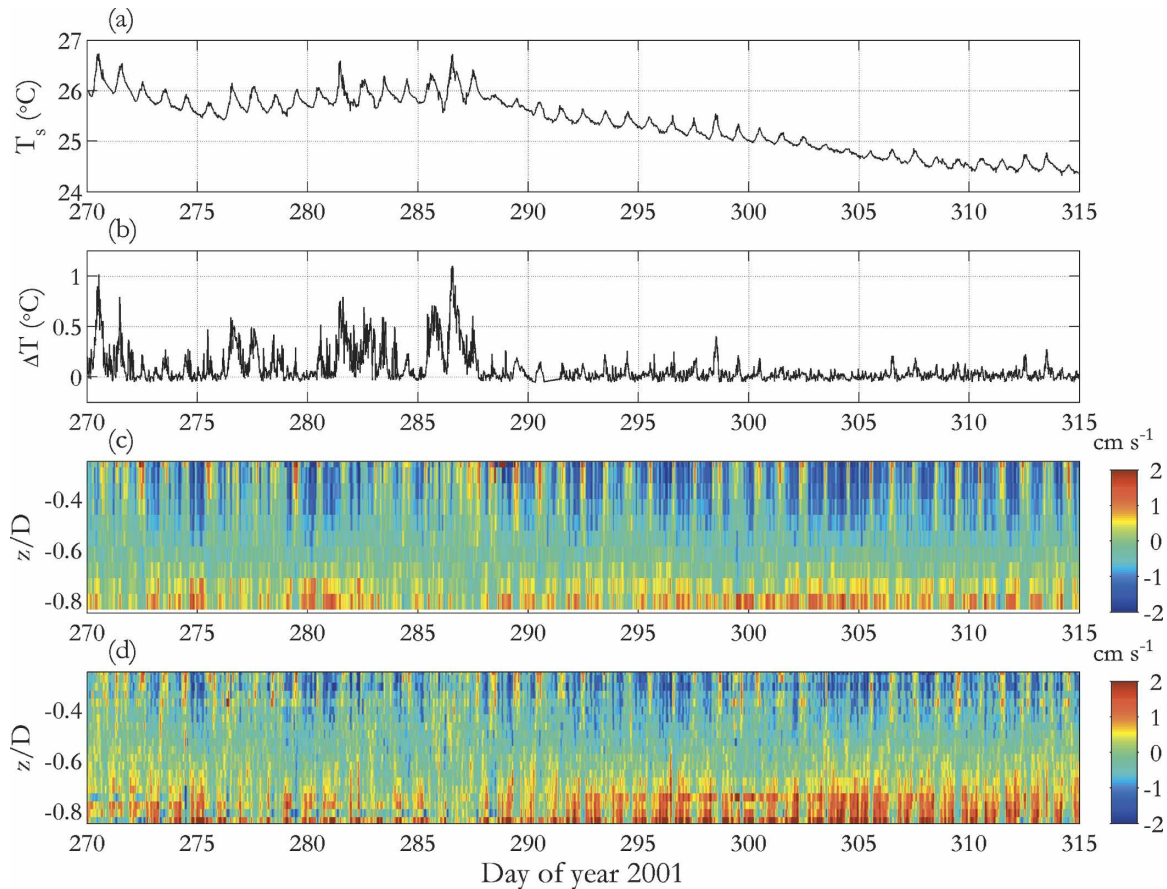


FIG. 5. For September–November 2001, (a) water surface temperature, (b) top–bottom temperature difference on the 16-m isobath, (c) cross-shore flow on the 8-m isobath, and (d) cross-shore flow on the 16-m isobath.

sumably, in the heating case, bottom mixing due to longshore flows along with convection associated with the always present evaporation was sufficient to maintain turbulence throughout most of the water column despite the weak stratification that formed during the heating phases. Unfortunately, although the heating flow was evident in all of the datasets, this was the only case in which we clearly observed it. Thus, for the rest of our discussion, we will focus on the properties of the cooling flows.

To test the generality of the result seen in Fig. 8a, we took all of our velocity data for cooling periods, and scaled each data point by its estimated top–bottom shear, ΔV . Echoing Phillips’s similarity theory, after scaling by ΔV , a single shape emerges for all of the cross-flow velocity profiles during cooling (Fig. 9). Note that ΔV can be thought of as fitting parameter that has been chosen to minimize the deviation of a given profile from the composite of all profiles. As intended, this procedure clarifies the vertical structure of the cooling flows, but leaves open the issue of how ΔV depends on

the various forcing parameters (e.g., u_* or u_f), system geometry (e.g., bottom slope β), and the periodic nature of the forcing.

The analysis given in section 2 suggest six possible scalings for ΔV depending on different choices for the momentum balance and for the thermal energy balance. These scalings are summarized in Table 1. As seen in Fig. 10, it is clear that the advective inertia scalings better collapse the data than do the viscous or unsteady scalings, and that the advective thermal energy balance is better than the unsteady balance. Support for the steady thermal balance, at least for cooling flows, comes from the autumn 2001 data, for which we found that the horizontal temperature difference and the cooling were in phase (see Fig. 7).

Thus, it would appear that overall the Phillips scaling (10) best fits our data, although the match is not perfect. In particular, ΔV appears to go to 0 for nonzero values of u_f . In part this may reflect the fact that the smallest values of u_f may come from times of strong heating and thus from times when nighttime cooling

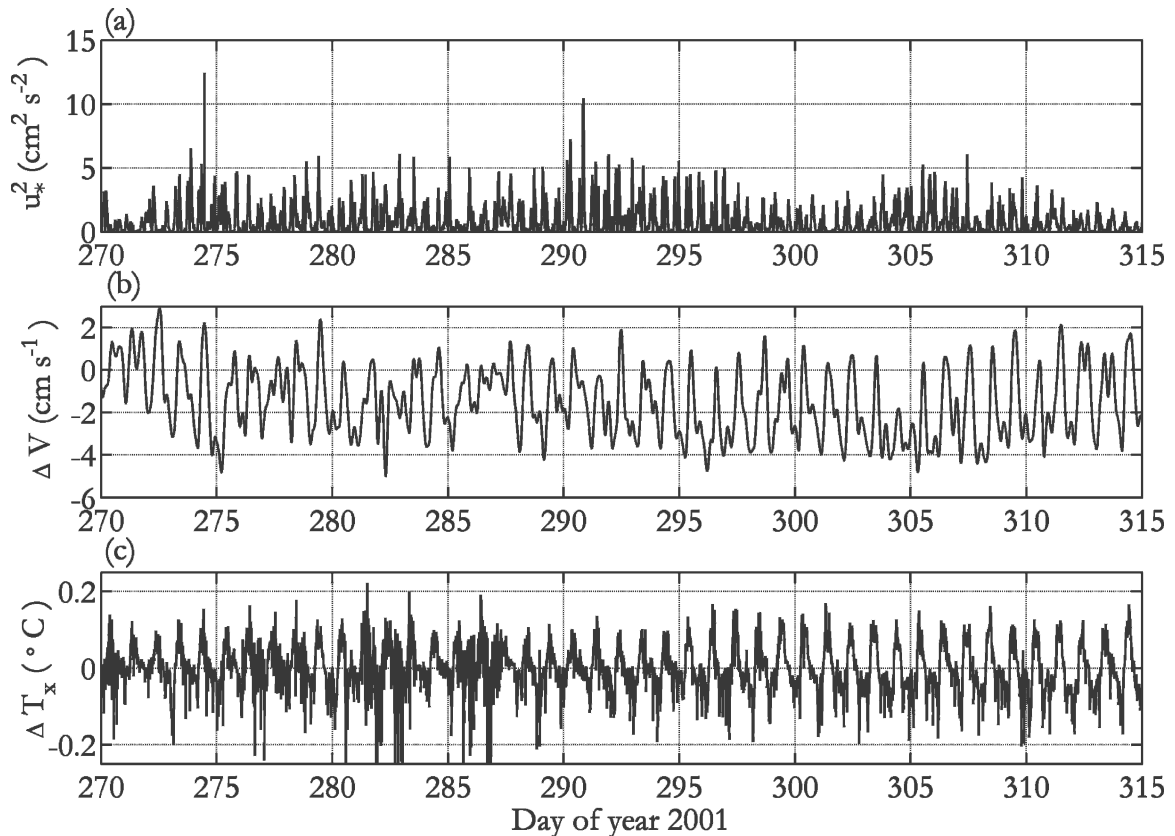


FIG. 6. (a) Estimated bottom stress u_*^2 , (b) top-bottom shear in cross-shore flow on the 16-m isobath, and (c) horizontal temperature differences between the 8- and 16-m isobaths measured at 8 m below the water surface.

may have just eliminated any near-surface stratification that had developed during daytime heating. This behavior also suggests that, for weak cooling, viscous stresses and unsteady effects may be important. This can be examined by looking at the how the scaled shear, $\beta^{1/3}\Delta V/u_f$, may depend on the relative size of the stress divergence and unsteadiness terms. These ratios are easily constructed from the scaling given in section 2, namely,

$$\frac{\text{advective inertia}}{\text{stress divergence}} \sim \left(\frac{u_f}{u_*}\right)\beta^{2/3} \quad (14)$$

and

$$\frac{\text{advective inertia}}{\text{unsteady inertia}} \sim \left(\frac{u_f T}{D}\right)\beta^{4/3}. \quad (15)$$

While there is considerable scatter in the plots of $\beta^{1/3}\Delta V/u_f$ as functions of these two parameters (Fig. 11), it is clear that when cooling is weak or when the longshore flow is strong, the cross-shore exchange flow is weakened. The effect of longshore flow is similar to that seen in estuarine flows, where the strongest gravi-

tational circulation is observed at neap tides (e.g., Hansen and Rattray 1965; Stacey et al. 2001). The effect of unsteadiness is also straightforward: if the buoyancy forcing changes quickly relative to the time needed to

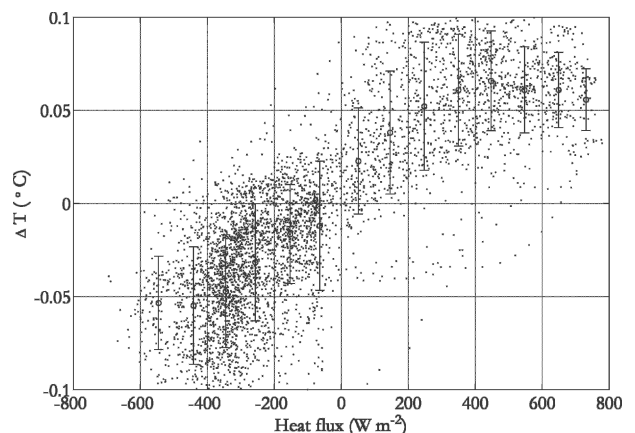


FIG. 7. Temperature difference at 8-m depth between the 8- and 16-m isobaths as a function of surface heating rate. The circles with error bars represent the results (with \pm standard deviations) of averaging the individual measurements in 100 W m^{-2} bins.

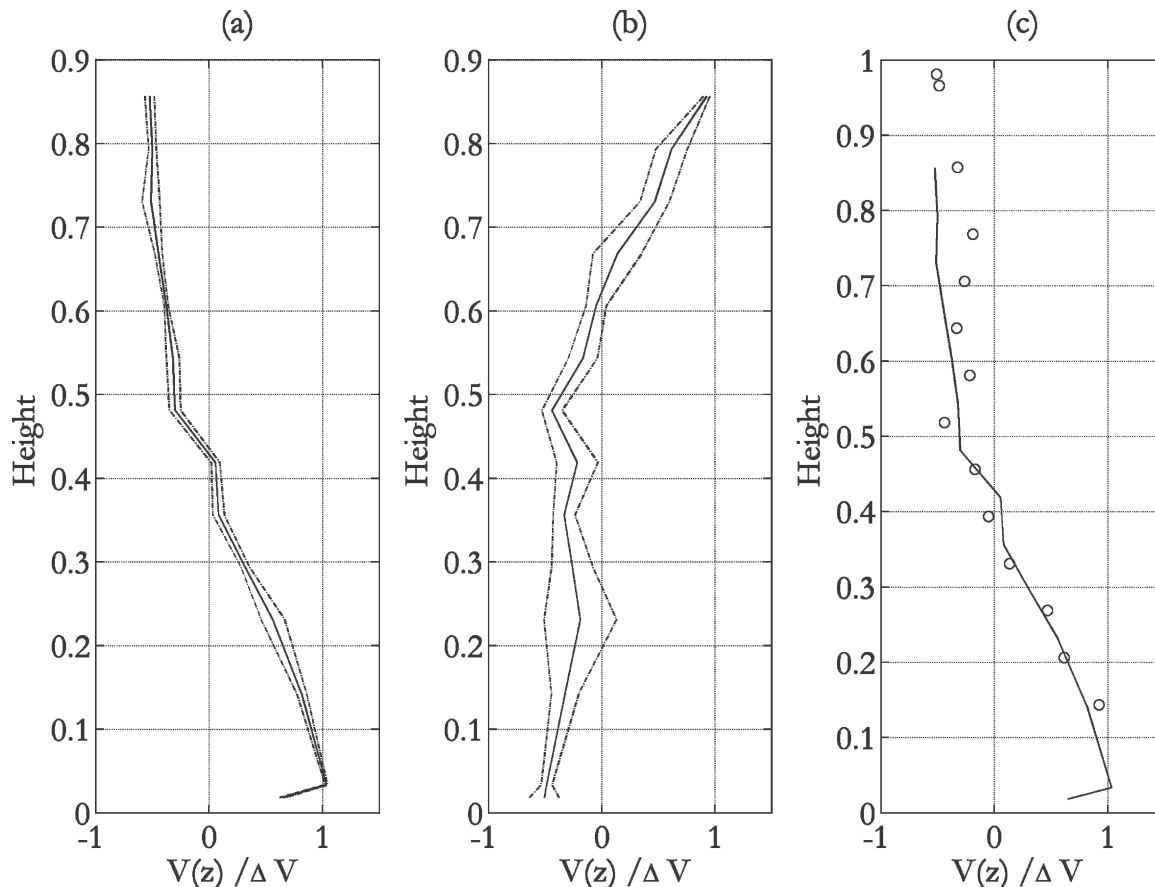


FIG. 8. Box-B velocity profiles scaled by top-bottom shear: (a) the average (solid) and standard deviation (dot-dash) of all cooling profiles, (b) the average (solid) and standard deviation (dot-dash) of all heating profiles, and (c) a comparison of the vertical structures of the cooling (solid line) and heating (open circles) flows. In (c) the heating flow profile has been flipped vertically so that it can be compared with the cooling flow.

establish the steady convective flow, the ensuing exchange will also be weaker (Farrow and Patterson 1993).

Thus, examination of the dependence of ΔV on u_f , u_* , T , D , and β suggests that the main dynamics are the inertial dynamics first described by Phillips for the Red Sea as a whole, although in the present case, it is clear that the variation of depth with distance from shore is also important. However, because longshore flows can enhance the vertical mixing of momentum and because the forcing is intrinsically unsteady, turbulent stress divergence and unsteadiness both play secondary roles in the cross-shore momentum balance.

Last, to show that our results are not exceptional, we compared them with those of Sturman et al. (1999). To do so, it is necessary to cast our results in terms of the 2D exchange flow, Q . After fitting all of the profile data with smoothing splines (de Boor 1974), one each for $z/D \leq -0.85$ and $z/D > -0.85$, we integrated the dimensionless profile seen in Fig. 9 numerically, finding that $Q \approx 0.15\Delta VD$ or $Q \approx 0.3u_f D$ (using $\Delta V/u_f \approx 2$).

In our case, $\beta \approx 0.2$, so that Sturman et al. (1999) would predict that $Q = 0.2u_f D$. The degree of agreement between our results and those of Sturman et al. is best seen by plotting our results, expressed in terms of Q ,

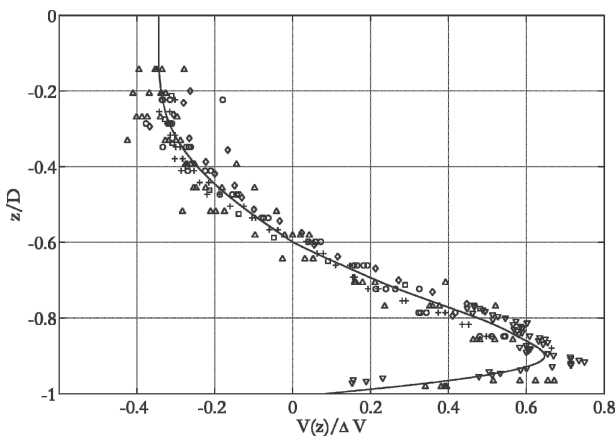


FIG. 9. Composite cross-shore flow profiles for all cooling periods: $V(z)$ scaled by top-bottom shear, ΔV .

TABLE 1. Possible scalings for ΔV .

Balance	Unsteady inertia	Stress divergence	Advective inertia
Steady temperature	$V_{US} \sim (u_f^3 T/D)^{1/2}$	$V_{VS} \sim (u_f^{3/2} q^{1/2})$	$V_{NS} \sim \beta^{-1/3} u_f$
Unsteady temperature	$V_{UU} \sim (\beta u_f^3 T^2/D_0^2)$	$V_{VU} \sim (\beta u_f^3 T/qD)$	$V_{NU} \sim (u_f^3 T/D)^{1/2}$

along with those presented in Sturman et al. (Fig. 12), where we have also added 95% confidence interval lines to their fit. Clearly the deviation of our observations from (13) is well within the scatter of the numerical, laboratory, and field results that Sturman et al. collated. Thus, the consistency of our results with previous laboratory and field work lends strong support for our interpretation of the measured flows being the result of an inertial flow driven by temperature gradients created topographically by surface heat fluxes.

6. Discussion and conclusions

Our field data from Eilat show thermally driven flows associated with temperature differences that de-

velop because of variations in depth. In summer heating conditions, daytime (heating) flows are offshore at the surface while nighttime (cooling) flows are offshore at depth. Velocity profiles measured during cooling are nearly self-similar with a top-bottom shear ΔV that is best represented by the Phillips scaling $\Delta V \sim \beta^{-1/3} u_f$. However, when u_f is small or longshore flows are strong, the implied constant of proportionality must be reduced from the value that might exist for a steady flow with no externally produced turbulence

To clarify the role of bottom-produced turbulence in regulating the exchange flow as well as the effects of unsteadiness, it would be useful to carry out a computational study in which one models a longshore flow in a wedge driven by an imposed barotropic pressure gra-

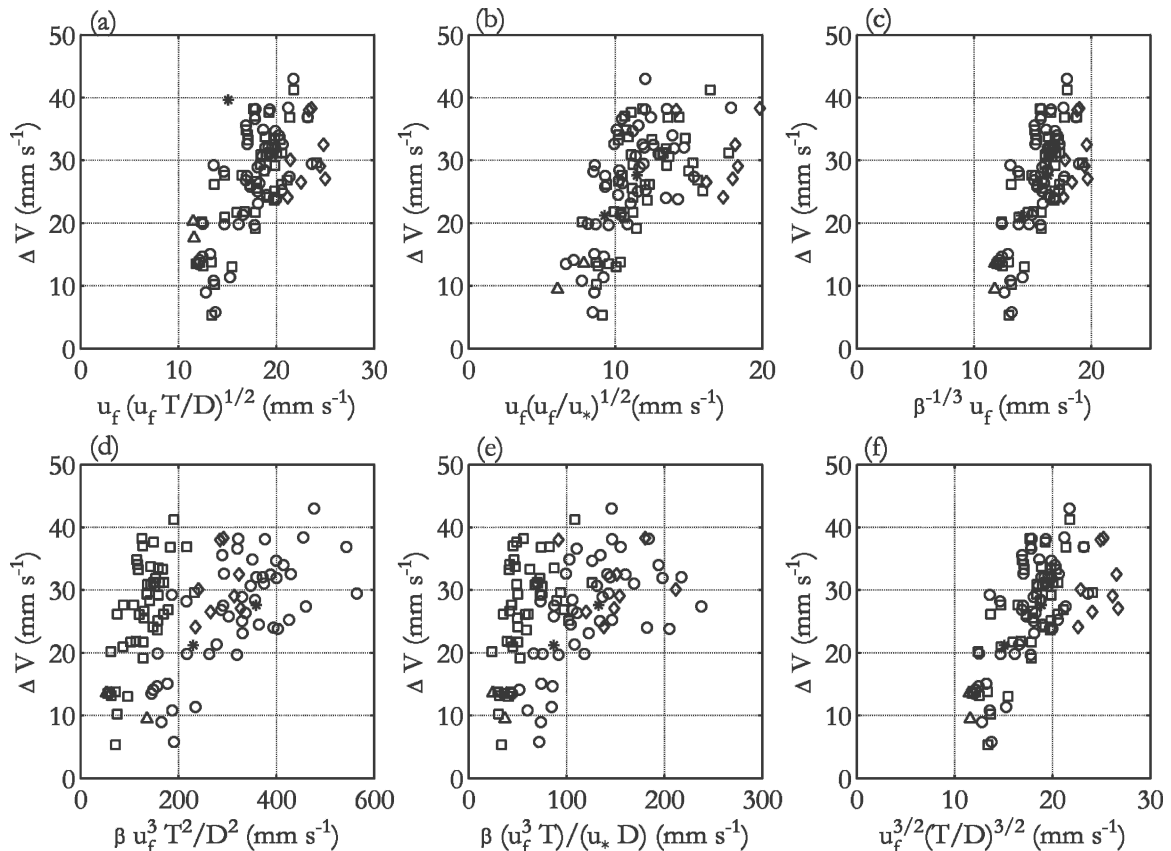


FIG. 10. Observed values of ΔV plotted as functions of different dimensional groups suggested by scaling. In (a)–(c) a steady balance is assumed for the thermal energy equation and also that the dominant term in the cross-shore momentum equation is (a) unsteady inertia, (b) stress divergence, and (c) steady inertia. In (d)–(f) an unsteady thermal energy balance is assumed and also that the dominant term in the cross-shore momentum equation is (d) unsteady inertia, (e) stress divergence, and (f) steady inertia.

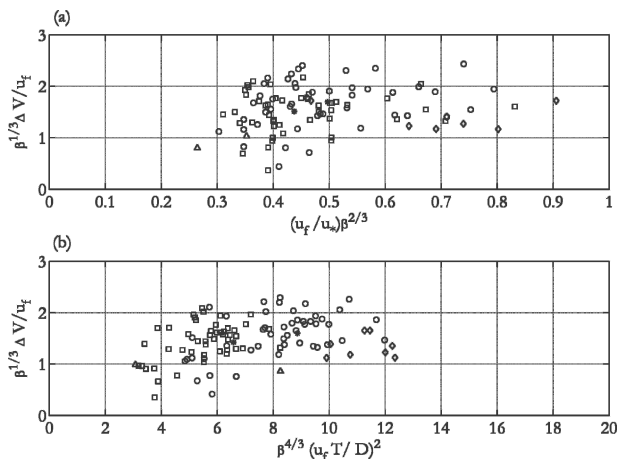


FIG. 11. ΔV made dimensionless by the inertial shear estimate and plotted as a function of (a) the ratio of the stress divergence to steady inertia terms and (b) the ratio of the steady to unsteady inertia terms.

dent at the same time as the surface of the wedge is cooled. The advantages of this approach are twofold. 1) It would be possible to examine the behavior of the exchange flow for $u_f/u_* < 1$, a condition we did not observe for any appreciable period of time in Eilat, and 2) it would also be possible to look at the pure cooling case, that is, the limit where $u_f/u_* \rightarrow \infty$; again this is a limit that we cannot observe easily in the field.

The buoyancy-driven flow we have described in this paper is a pronounced feature of the nearshore environment of Eilat, being present at all times of year. Neiman et al. (2004) suggest that cooling flows similar to what we observe, but on the eastern shore of the Gulf of Aqaba, are likewise commonplace. Since all that is required for the thermal siphon to work is that the depth be variable, we expect it to be a generic feature of the nearshore coastal ocean, especially where slopes are pronounced or where shallow regions connect to deeper regions. For example, in Eilat, north of the Steinitz laboratory, there is a shallow coral reef lagoon that connects with deeper water via several channels. Based on our present results, we should expect that thermally driven flows associated with differential heating and cooling might be the dominant means of promoting exchange between the lagoon and the Gulf of Aqaba, although, in this case the flow rate might be set by internal hydraulic controls (cf. Armi 1986) in the narrow passes out of the lagoon.

It is important to assess the generality of the mechanism we observed; that is, is the thermal siphon likely to be important generally for coral reefs or other near-shore environments? First, while the heat losses we cal-

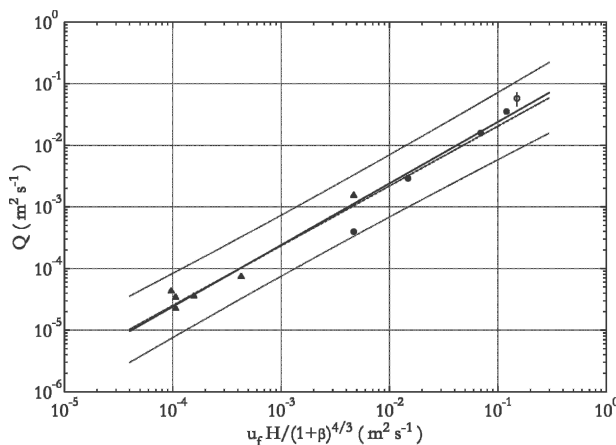


FIG. 12. Synthesis of laboratory, numerical, and field observations of cooling over a slope for laboratory and numerical experiments (filled triangles), previous field experiments (filled circles), and flows on the Eilat reef (open circles, vertical bar indicates the range of flows observed). The previous results have been redrawn from Sturman et al. (1999). Sturman et al.'s fit is shown as a solid line, whereas a fit of the log of the observed flow as a function of the log of the predicted scaled flow is given as a dashed line with 95% confidence intervals shown as thin lines to either side.

culate for Eilat, typically 400 W m^{-2} , are larger than are commonly seen at most coastal environments, the $1/3$ -power dependency of u_f on the heat flux means that a more typical cooling rate of 200 W m^{-2} will still produce flows that are 80% as strong as what we observe here. Second, these flows can only take place shoreward of where the thermocline shoals, because offshore of this point surface heating and cooling will uniformly change the upper mixed layer temperature.

Third, while the topography of the Eilat reef is relatively simple, more complicated bathymetry including ridges and grooves, that is, deeper channels, is found on many reefs (see, e.g., Roberts et al. 1975). Since baroclinic pressure gradients increase with depth, longshore variations in depth should lead to longshore variations in the exchange flow, with stronger flows down the deeper grooves and weaker flows over the shallower ridges than we have observed in Eilat.

Fourth, there is the issue of waves. Much of the extant literature on coral reefs focuses on wave-driven flows. Yet for many reefs, for example, the interior lagoons and leeward sides of atolls, waves are not likely to be important.² Even when waves are present, they

² A nice example of this can be seen in the September 2004 issue of *National Geographic* in which a photo of Male, the capital of the Maldives and a coral atoll, is printed. Breaking waves can be seen for approximately 25% of the coastline whereas the other 75% is wave free.

might not force strong flows. For example, on a typical fore reef offshore of where the waves break, the divergence of the wave radiation stress, the principal influence of the waves on the mean flow, may be small, such that even energetic surface waves may only weakly influence onshore–offshore exchanges. Second, since the radiation stress divergence acts like a depth-independent body force (e.g., Hearn 1999), it can be offset by barotropic pressure gradients produced by raising or lowering the free surface, much like what happens on a beach.

Thus, it seems worthwhile to consider the possibility for any reef of interest that convective flows might be important, even if their contribution to net transport may at times be swamped by surface wave effects, by cross-shore winds (Tapia et al. 2004), or by internal wave shoaling as observed by Leichter et al. (1996, 2003) for the Florida Keys. Even in this last case, given that much of the reef exists on a steep slope extending from the surface to nearly 80 m, and that Hawk Channel, which is shoreward of the reef crest, is relatively shallow, one might expect thermal flows at times. An important difference between Eilat and the Florida Keys is the fact that longshore flows in the Florida Keys are often stronger than what we observe at Eilat (J. Leichter 2005, personal communication), which would tend to suppress the buoyancy-driven flow. In this regard, an energetic environment like the Florida Keys might provide a good test of the scaling in the limit where u_f/u_* tends to zero. Likewise, one can imagine that in a given case, even if waves are not responsible for forcing mean flows, they may still modulate the convective exchange by increasing u_* (Hearn 1999).

We emphasize that what we describe here is fundamentally a nearshore process. At larger scales, the cross-shore flows will be strongly influenced by rotation such that for distances offshore of the order of the Rossby radius or larger, the cooling flow must turn parallel to the shore with continued downslope flow presumably confined to near-bottom Ekman layers (Symonds and Gardiner-Garden 1994; Pringle 2001). Additionally, for larger-scale shelf flows, there is the additional complexity associated with the fact that the heat transfer itself is partially determined by the evolving temperature field on the shelf, whereas, for the present case, there is little spatial variation in the heat flux because the horizontal temperature gradients, albeit dynamically significant, are relatively small.

Nonetheless, we believe that the “thermal siphon” we describe here represents an important class of flow for fringing reefs and should be accounted for in any

attempt to model their hydrodynamics or to evaluate their biogeochemical functioning.

Acknowledgments. The authors are grateful to Moti Ohavia, Inbal Ayalon, Yaron Shiff, Eaton Dunkleberger, and Greg Shellenbarger, all of whom helped with the field work we described in this paper. We also acknowledge an anonymous referee who rightfully challenged our original interpretation of our data. This work was supported by the U.S.–Israel Binational Science Foundation, by funding from the Stanford University Bio-X initiative, and by NSF Grants OCE 9907110 and OCE 0117859. MAR is grateful for support in the form of a fellowship from the Stanford Graduate Fellowship program.

APPENDIX

Scaled Momentum and Buoyancy Balances

The scaling discussed in section 2 and tested in section 4 using our field data can be easily derived through consideration of the 2D governing equations for momentum and buoyancy:

$$\frac{\partial V}{\partial t} + V \frac{\partial V}{\partial y} + W \frac{\partial V}{\partial z} = -\frac{1}{\rho_0} \frac{\partial P}{\partial y} + \frac{\partial}{\partial z} \left(v_t \frac{\partial V}{\partial z} \right), \quad (\text{A1})$$

$$\frac{\partial W}{\partial t} + V \frac{\partial W}{\partial y} + W \frac{\partial W}{\partial z} = -\frac{1}{\rho_0} \frac{\partial P}{\partial z} - B + \frac{\partial}{\partial z} \left(v_t \frac{\partial W}{\partial z} \right), \quad (\text{A2})$$

$$\frac{\partial B}{\partial t} + V \frac{\partial B}{\partial y} + W \frac{\partial B}{\partial z} = -\frac{\partial \tilde{B}}{\partial z}, \quad \text{and} \quad (\text{A3})$$

$$B = -\alpha g(\theta - \theta_0), \quad (\text{A4})$$

where \tilde{B} is the vertical buoyancy flux and W is the vertical velocity. The other symbols are defined in section 2. Note that \tilde{B} includes the effects of both short-wave radiation and turbulent mixing; at the water surface,

$$\tilde{B}(z=0) = -\frac{\alpha g \tilde{H}}{\rho_0 c_p} = -\frac{u_f^3}{D} = -B_0. \quad (\text{A5})$$

We start by using the inertial scaling as the basis for the rest of what follows; in which case,

$$y = \beta^{-1} D y^*, \quad z = D y^*, \quad t = T t^*,$$

$$V = \beta^{-1/3} u_f V^*, \quad W = \beta^{2/3} u_f W^*,$$

$$P = \rho_0 \beta^{-2/3} u_f^2 P^*, \quad \text{and} \quad B = \beta^{-2/3} u_f^2 D^{-1} B^*,$$

where the superscript asterisk refers to dimensionless variables. Using these definitions, the governing equations become

$$\frac{D}{\beta^{2/3}u_f T} \frac{\partial V^*}{\partial t^*} + \left(V^* \frac{\partial V^*}{\partial y^*} + W^* \frac{\partial V^*}{\partial z^*} \right) = \frac{q}{\beta^{2/3}u_f} \frac{\partial}{\partial z^*} \left(v_t^* \frac{\partial V^*}{\partial z^*} \right) - \frac{\partial P^*}{\partial y^*}, \tag{A6}$$

$$\frac{\beta^{4/3}D}{u_f T} \frac{\partial W^*}{\partial t^*} + \beta^2 \left(V^* \frac{\partial W^*}{\partial y^*} + W^* \frac{\partial W^*}{\partial z^*} \right) = \frac{\beta^{4/3}q}{u_f} \frac{\partial}{\partial z^*} \left(v_t^* \frac{\partial W^*}{\partial z^*} \right) - \frac{\partial P^*}{\partial z^*} - B^*, \text{ and} \tag{A7}$$

$$\frac{D}{\beta^{2/3}u_f T} \frac{\partial B^*}{\partial t^*} + V^* \frac{\partial B^*}{\partial y^*} + W^* \frac{\partial B^*}{\partial z^*} = - \frac{\partial B^*}{\partial z^*}. \tag{A8}$$

Note that as long as $\beta \ll 1$, the pressures will be hydrostatic. For $\beta \ll 1$, the purely inertial (Phillips 1966) scaling should only apply when

$$\frac{D}{\beta^{2/3}u_f T} \ll 1 \quad \text{and} \quad \frac{q}{\beta^{2/3}u_f} \ll 1.$$

The first condition can be met for small β so long as $(u_f T/D) \gg \beta^{-2/3}$, that is, that the convective mixing time scale (D/u_f) is much less than the time scale over which the buoyancy flux varies.

However, for scaling alone, the second condition cannot be satisfied for $\beta < 1$ since $q \geq u_f$. This suggests that as a first approximation the momentum and buoyancy balances should be

$$\left(V^* \frac{\partial V^*}{\partial y^*} + W^* \frac{\partial V^*}{\partial z^*} \right) = \frac{q}{\beta^{2/3}u_f} \frac{\partial}{\partial z^*} \left(v_t^* \frac{\partial V^*}{\partial z^*} \right) - \frac{\partial P^*}{\partial y^*}, \tag{A9}$$

$$0 = - \frac{\partial P^*}{\partial z^*} - B^*, \text{ and} \tag{A10}$$

$$V^* \frac{\partial B^*}{\partial y^*} + W^* \frac{\partial B^*}{\partial z^*} = - \frac{\partial B^*}{\partial z^*}. \tag{A11}$$

This set of equations is identical to the ones solved by Tragou and Garrett (1997) for the case of buoyancy-driven flows in closed basins like the Red Sea. As discussed by Tragou and Garrett (1997), the Phillips (1966) similarity solution for the inviscid equations can be retained if particular forms are chosen for the eddy viscosity and diffusivity. Interestingly, for $D = \beta y$, it can be shown that the Phillips similarity solution also applies, except that the governing ordinary differential equations are considerably more complicated than those studied by Tragou and Garrett (1997) and Phillips (1966). While the solution of these equations is beyond the scope of the present paper, formally, (24)–(26) show that for the steady case we should expect the functional relationship

$$\begin{aligned} V^* &= (B_0 y)^{1/3} V^* \left(\frac{z}{D}, \beta^{-2/3} \frac{q}{u_f} \right) \\ &= (B_0 y)^{1/3} V^* \left(\frac{z}{D}, \beta^{-2/3} \frac{u_*}{u_f} \right) \end{aligned}$$

to hold. The data presented in sections 3 and 4 suggest that this can be separated as

$$V = (B_0 y)^{1/3} F \left(\beta^{-2/3} \frac{u_*}{u_f} \right) G \left(\frac{z}{D} \right), \tag{A12}$$

where F and G are dimensionless functions of their respective arguments.

In a similar vein, we can examine the Farrow and Patterson (1993) analysis. If we assume a viscous–buoyancy balance and that unsteadiness balances the vertical buoyancy flux,

$$V = \frac{\beta u_f^3 T}{q D} V^*, \quad W = \frac{\beta^2 u_f^3 T}{q D} W^*,$$

$$B = \frac{u_f^3 T}{D^2} B^*, \quad \text{and} \quad P = \rho_0 \frac{u_f^3 T}{D},$$

then the y momentum and buoyancy balances read

$$\begin{aligned} \frac{D}{q T} \frac{\partial V^*}{\partial t^*} + \frac{\beta^2 u_f^3 T}{q^2 D} \left(V^* \frac{\partial V^*}{\partial y^*} + W^* \frac{\partial V^*}{\partial z^*} \right) = \\ - \frac{\partial P^*}{\partial y^*} + \frac{\partial}{\partial z^*} \left(v_t^* \frac{\partial V^*}{\partial z^*} \right) \quad \text{and} \end{aligned} \tag{A13}$$

$$\frac{\partial B^*}{\partial t^*} + \beta^2 \left(\frac{u_f}{q} \right)^3 \left(\frac{q T}{D} \right)^2 \left(V^* \frac{\partial B^*}{\partial y^*} + W^* \frac{\partial B^*}{\partial z^*} \right) = - \frac{\partial \tilde{B}^*}{\partial z^*}. \tag{A14}$$

If $\beta \ll (D/qT)^{1/2}$, the nonlinear terms can be discarded and analytical solutions describing the unsteady viscous flow can be found by standard means (Farrow and Patterson 1993). For example, if $D \ll qT$, then a

quasi-steady viscous flow results, with the unsteadiness arising from unsteadiness in the buoyancy flux.

Note that the strength of the viscous flow can be modulated by turbulence produced by the longshore flow: When longshore currents are strong, $q \sim u_*$ must hold and thus, since $q > u_f$, the exchange flow will weaken. Conversely, the strongest exchange flows should exist when the longshore flow is weak or even nonexistent as in the experiments of Sturman et al. (1999).

Last, when $\beta \ll (D/qT)^{1/2}$ and $(u_f/q) = O(1)$, that is, when the slope is sufficiently steep and turbulence generated by the longshore flow is not too strong, advection should dominate and the Phillips (1966) scaling should be appropriate.

REFERENCES

- Armi, L., 1986: The hydraulics of two layers with different densities. *J. Fluid Mech.*, **163**, 27–58.
- Assaf, G., and J. Kessler, 1976: Climate and energy exchange in the Gulf of Aqaba. *Mon. Wea. Rev.*, **104**, 381–385.
- Atkinson, M., S. V. Smith, and E. D. Stroup, 1981: Circulation in Enewetak Atoll lagoon. *Limnol. Oceanogr.*, **26**, 1074–1083.
- Baird, M., and M. J. Atkinson, 1997: Measurement and prediction of mass transfer to coral reefs. *Limnol. Oceanogr.*, **42**, 1685–1693.
- Benayahu, Y., and Y. Loya, 1977: Space partitioning by stony corals and benthic algae on the coral reefs of the northern Gulf of Eilat (Red Sea). *Helgol. Meeresunters.*, **30**, 362–382.
- Berman, T., N. Paldor, and S. Brenner, 2000: Simulation of wind-driven circulation in the Gulf of Elat (Aqaba). *J. Mar. Syst.*, **26**, 349–365.
- , —, and —, 2003: The seasonality of tidal circulation in the Gulf of Aqaba. *Isr. J. Earth Sci.*, **52**, 11–19.
- Boden, B. P., 1952: Natural conservation of insular plankton. *Nature*, **169**, 697–699.
- Checkley, D. M., Jr., S. Raman, G. L. Maillet, and K. M. Mason, 1988: Winter storm effects on the spawning and larval drift of a pelagic fish. *Nature*, **335**, 346–348.
- de Boer, C., 1978: *A Practical Guide to Splines*. Springer-Verlag, 346 pp.
- Fairall, C. W., E. F. Bradley, D. P. Rogers, J. B. Edson, and G. S. Young, 1996: Bulk parameterization of the air–sea fluxes for Tropical Ocean Global Atmosphere Coupled–Ocean Atmosphere Response Experiment. *J. Geophys. Res.*, **101**, 3747–3764.
- Falter, J. L., 2003: Mass transfer limits to nutrient uptake by shallow coral reef communities. Ph.D. thesis, University of Hawaii, 126 pp.
- Farrow, D. E., and J. C. Patterson, 1993: On the response of a reservoir sidearm to diurnal heating and cooling. *J. Fluid Mech.*, **246**, 143–161.
- Fischer, H. B., E. J. List, R. C. Y. Koh, J. Imberger, and N. H. Brooks, 1979: *Mixing in Inland and Coastal Waters*. Academic Press, 483 pp.
- Fishelson, L., 1971: Ecology and distribution of the benthic fauna in the shallow waters of the Red Sea. *Mar. Biol.*, **10**, 113–133.
- Genin, A., and N. Paldor, 1998: Changes in the circulation and current spectrum near the tip of the seasonally mixed Gulf of Eilat. *Isr. J. Earth Sci.*, **47**, 87–92.
- , G. Yahel, M. A. Reidenbach, J. R. Koseff, and S. G. Monismith, 2002: Intense benthic grazing on phytoplankton in coral reefs revealed using the control volume approach. *Oceanography*, **15**, 90–96.
- Gordon, L., A. Lohrmann, and T. Jones, 1998: Internal wave generation in lakes with very slow flow. *Proc. Sixth Working Conf. on Current Measurement*, San Diego CA, IEEE, 212–215.
- Gross, T. F., and F. E. Werner, 1994: Residual circulations due to bottom roughness variability under tidal flows. *J. Phys. Oceanogr.*, **24**, 1494–1502.
- Hansen, D. V., and M. Rattray Jr., 1965: Gravitational circulation in straits and estuaries. *J. Mar. Res.*, **23**, 104–122.
- Hatcher, B. G., 1997: Coral reef ecosystems: How much greater than the whole is the sum of the parts? *Coral Reefs*, **12** (Suppl.), 577–591.
- Hearn, C. J., 1999: Wave-breaking hydrodynamics within coral reef systems and the effect of changing relative sea level. *J. Geophys. Res.*, **104**, 30 007–30 019.
- Jacobs, P., and G. N. Ivey, 1999: Rossby number regimes for isolated convection in a homogeneous rotating fluid. *Dyn. Atmos. Oceans*, **30**, 149–171.
- Kraines, S. B., T. Yanagi, M. Isobe, and H. Komiyama, 1998: Wind–wave driven circulation on the coral reef at Bora Bay, Miyako Island. *Coral Reefs*, **17**, 133–143.
- Leichter, J. J., S. R. Wing, S. L. Miller, and M. W. Denny, 1996: Pulsed delivery of sub-thermocline water to Conch Reef (Florida Keys), by internal tide bores. *Limnol. Oceanogr.*, **41**, 1490–1501.
- , H. L. Stewart, and S. L. Miller, 2003: Episodic nutrient transport to Florida coral reefs. *Limnol. Oceanogr.*, **48**, 1394–1407.
- Lentz, S., R. T. Guza, S. Elgar, F. Feddersen, and T. H. C. Hebers, 1999: Momentum balances on the North Carolina inner shelf. *J. Geophys. Res.*, **104**, 18 205–18 226.
- Lowe, R. J., J. L. Falter, M. D. Bandet, G. Pawlak, M. J. Atkinson, S. G. Monismith, and J. R. Koseff, 2005: Spectral wave dissipation over a barrier reef. *J. Geophys. Res.*, **110**, C04001, doi:10.1029/2004JC002711.
- Lugo-Fernandez, A., H. H. Roberts, W. J. Wiseman Jr., and B. L. Carter, 1998: Water level and currents of tidal and infragravity periods at Tague Reef, St. Croix (USVI). *Coral Reefs*, **17**, 343–349.
- Monismith, S. G., and A. Genin, 2004: Tides and sea level in the Gulf of Aqaba (Eilat). *J. Geophys. Res.*, **109**, C04015, doi:10.1029/2003JC002069.
- , J. Imberger, and T. Morrissey, 1990: Horizontal convection in the sidearm of a small reservoir. *Limnol. Oceanogr.*, **35**, 1676–1702.
- Munk, W. M., G. C. Ewing, and R. R. Revelle, 1949: Diffusion in Bikini Lagoon. *Trans. Amer. Geophys. Union*, **30**, 159–166.
- Neiman, H., C. Richter, H. Jonkers, and M. I. Badran, 2004: Red Sea gravity currents cascade near-reef phytoplankton to the twilight zone. *Mar. Ecol. Progr. Ser.*, **269**, 91–99.
- Pawlowicz, R., B. Beardsey, S. Lentz, E. Dever, and A. Anis, 2001: Software simplifies air–sea data estimates. *Eos, Trans. Amer. Geophys. Union*, **82**, 2.
- Phillips, O. M., 1966: On turbulent convection currents and the circulation of the Red Sea. *Deep-Sea Res.*, **13**, 1149–1160.
- Pringle, J. M., 2001: Cross-shelf eddy heat transport in a wind-free coastal ocean. *J. Geophys. Res.*, **106**, 2589–2604.

- Reidenbach, M. A., 2004: Boundary layer dynamics in coral reef systems. Ph.D. thesis, Stanford University, 263 pp.
- Roberts, H. H., S. P. Murray, and J. H. Suhayda, 1975: Physical process in a fringing reef system. *J. Mar. Res.*, **33**, 233–260.
- Spigel, R. H., J. Imberger, and K. N. Rayner, 1986: Modeling the diurnal mixed layer. *Limnol. Oceanogr.*, **31**, 533–556.
- Stacey, M. T., J. R. Burau, and S. G. Monismith, 2001: Creation of residual flows in a partially stratified estuary. *J. Geophys. Res.*, **106**, 17 013–17 038.
- Storlazzi, C. D., M. A. McManus, and J. D. Figurski, 2003: Long-term, high frequency current and temperature measurements along central California; insights into upwelling/relaxation and internal waves on the inner shelf. *Cont. Shelf Res.*, **23**, 901–918.
- Sturman, J. J., C. E. Oldham, and G. N. Ivey, 1999: Steady convective exchange down slopes. *Aquat. Sci.*, **61**, 260–278.
- Symonds, G., and R. Gardiner-Garden, 1994: Coastal density currents forced by cooling events. *Cont. Shelf Res.*, **14**, 143–157.
- , K. P. Black, and I. R. Young, 1995: Wave-driven flow over shallow reefs. *J. Geophys. Res.*, **100**, 2639–2648.
- Tapia, F. J., J. Pineda, F. J. Ocampo-Torres, H. Fuchs, P. E. Parnell, P. Montero, and S. Ramos, 2004: High-frequency observations of wind-forced onshore transport at a coastal site in Baja California. *Cont. Shelf Res.*, **24**, 1573–1585.
- Tragou, E., and C. J. R. Garrett, 1997: The shallow thermohaline circulation of the Red Sea. *Deep-Sea Res.*, **44**, 1355–1376.
- von Arx, W. S., 1954: Circulation systems of Bikini and Rongelap lagoons, Bikini and nearby atolls, Marshall Islands. U.S. Geological Survey Prof. Paper 260-B, 265–291.
- Wolanski, E., 1987: Some evidence for boundary mixing near coral reefs. *Limnol. Oceanogr.*, **32**, 735–739.
- Wolf-Vecht, A., N. Paldor, and S. Brenner, 1992: Hydrographic indications of advection/convection effects in the Gulf of Elat. *Deep-Sea Res.*, **39**, 1393–1401.
- Yahel, G., A. F. Post, K. Fabricius, D. Marie, D. Vaultot, and A. Genin, 1998: Phytoplankton distribution and grazing near coral reefs. *Limnol. Oceanogr.*, **4**, 551–563.
- Yahel, R., G. Yahel, and A. Genin, 2002: Daily cycles of suspended sand in coral reefs: a biological control. *Limnol. Oceanogr.*, **47**, 1071–1083.